ORIGINAL PAPERS

Influence of the PHY domain on the ms-photoconversion dynamics of a knotless phytochrome
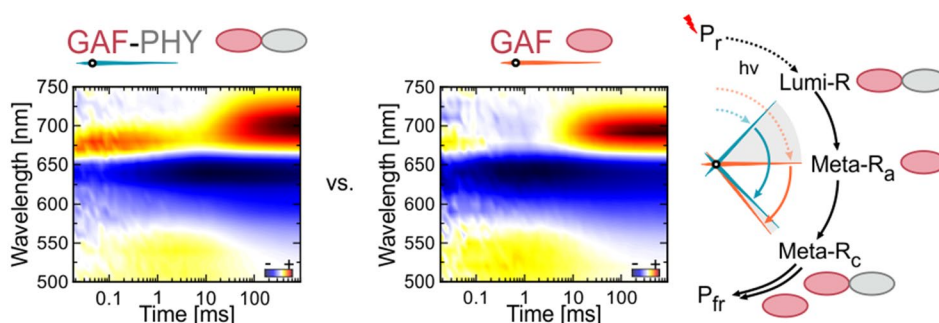
Tobias Fischer[1] · Lisa Köhler[2] · Tanja Ott[1] · Chen Song[2] · Josef Wachtveitl[1] · Chavdar Slavov[1]

Abstract

The ability of some knotless phytochromes to photoconvert without the PHY domain allows evaluation of the distinct effect of the PHY domain on their photodynamics. Here, we compare the *ms* dynamics of the single GAF domain (g1) and the GAF-PHY (g1g2) construct of the knotless phytochrome All2699 from cyanobacterium *Nostoc punctiforme*. While the spectral signatures and occurrence of the intermediates are mostly unchanged by the domain composition, the presence of the PHY domain slows down the early forward and reverse dynamics involving chromophore and protein binding pocket relaxation. We assign this effect to a more restricted binding pocket imprinted by the PHY domain. The photoproduct formation is also slowed down by the presence of the PHY domain but to a lesser extent than the early dynamics. This indicates a rate limiting step within the GAF and not the PHY domain. We further identify a pH dependence of the biphasic photoproduct formation hinting towards a pKa dependent tuning mechanism. Our findings add to the understanding of the role of the individual domains in the photocycle dynamics and provide a basis for engineering of phytochromes towards biotechnological applications.

Graphical abstract

Keywords Knotless phytochrome · Photochemistry · Time-resolved spectroscopy · Flash photolysis

✉ Josef Wachtveitl
  wveitl@theochem.uni-frankfurt.de

✉ Chavdar Slavov
  chslavov@theochem.uni-frankfurt.de

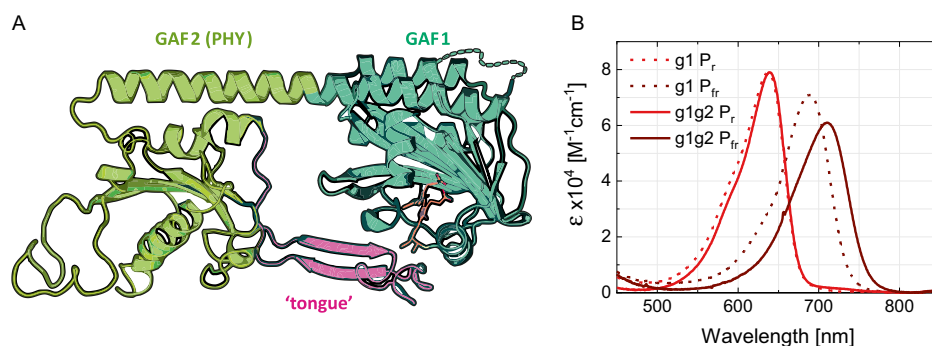Extended author information available on the last page of the article

1 Introduction

The photoreceptor superfamily of phytochromes is involved in the regulation of a variety of biologically relevant processes like photomorphogenesis, photoprotection and phototaxis in a multitude of different organisms [1, 2]. Their regulatory function is based on the photoconversion between a dark-adapted and a light-adapted state. Specifically, irradiation induces Z ↔ E isomerization of the embedded, covalently bound bilin chromophore that in turn triggers

Fig. 1 A Schematic drawing of the structural homology model of the P_r state of All2699g1g2. The homology model is based on the crystal structure of the All2699g1 domain (PDB ID 6OZA) [19] and the crystal structure of the structurally similar knotless phytochrome *Syn*Cph2 (PDB ID 4BWI) [22]. The PHY-like GAF2 domain (yellow) interacts with the chromophore (orange) embedded in the GAF1 domain (green) via the tongue-like protrusion displayed in pink. Taken from [23]. **B** Stationary absorption spectra of the P_r and P_{fr} state in All2699g1 (dotted lines) and All2699g1g2 (solid lines). The method to obtain the pure spectrum of the P_{fr} state was described elsewhere in detail [18]

formation of further intermediates characterized by reorganization of the protein scaffold.

Phytochromes can be divided into three groups based on the domain structure and composition of their photosensory core module (PCM). The PCM of Group I phytochromes, comprising canonical plant (e.g. *Oat*PhyA), bacterial (e.g. Agp1, *Dr*BphP), cyanobacterial (e.g. CphA, *Syn*Cph1) and fungal phytochromes (e.g. FphA, *Nc*Fph1), consists of a PAS-GAF-PHY array [3–5]. Group II phytochromes, known as knotless phytochromes, lack the PAS domain with its domain specific figure-of-eight knot formation with the GAF domain [1, 2, 6, 7], while Group III phytochromes, called cyanobacteriochromes (CBCRs), consist only of GAF domains [8]. So far, the latter two groups are found only in cyanobacteria [1]. In contrast to CBCRs, which cover the whole near-IR to UV spectral range, Group I and Group II phytochromes mainly switch between P_r (red-absorbing) and P_{fr} (far-red-absorbing) states [9–17].

Some knotless phytochromes retain their photoconversion abilities even in their isolated GAF domain (after removal of the PHY domain), and thus can be utilized as model systems to investigate the influence of the PHY domain on the photoconversion process [18, 19]. This is of particular interest since the PHY domain interacts directly with the chromophore embedded in the GAF domain via a structural element referred to as "tongue" (Fig. 1A). The latter undergoes secondary structure reorganization during photoconversion [6, 7]. This reorganization not only affects the slower, protein driven dynamics of the later intermediates in the photocycle, but also plays a key role in the signal transduction towards the output domain [20, 21].

The forward ($P_r \rightarrow P_{fr}$) reaction in the photocycle of canonical phytochromes typically involves three intermediates termed Lumi-R, Meta-R_a and Meta-R_c. The Lumi-R intermediate is formed directly after the decay of the excited state on the timescale of tens to hundreds of *ps* [24]. It contains the isomerized chromophore and a reorganized hydrogen-bonding network. Some studies distinguish Lumi-R_I and Lumi-R_{II} intermediates [24–29]. The structural changes in Lumi-R_I occur on the *ps* timescale and are limited to the ring D vicinity, while the following hydrogen bonding reorganization and structural changes in the wider vicinity of the chromophore are attributed to Lumi-R_{II} [24, 28, 29]. On the *μs* timescale, Lumi-R converts into the Meta-R_a intermediate via relaxation of the strained chromophore [21, 26, 27, 30–32]. Within a few *ms*, in plant and some cyanobacterial and bacterial phytochromes, the chromophore undergoes deprotonation to form the Meta-R_c intermediate [30, 31, 33, 34], which then forms the final state, P_{fr}, upon re-protonation of the chromophore on the tens to hundreds of *ms* timescale [21, 26, 27, 30–32]. However, the de-/re-protonation steps of the chromophore are not observed in all phytochromes, and thus the role of this mechanism in the dynamics of Meta-R_c is still under debate [24]. This formation of P_{fr} involves large-scale protein changes required for the final accommodation of the isomerized chromophore, reorganization of the hydrogen-bonding network and refolding of the tongue [20, 21, 24, 32]. In *Syn*Cph1 and *Oat*PhyA, this transition has been observed to be biphasic [27, 30].

Generally, the reverse photoconversion reaction ($P_{fr} \rightarrow P_r$) proceeds via two intermediates – Lumi-F and Meta-F. The Lumi-F intermediate contains an isomerized chromophore and is directly formed by the ultrafast photoreaction on the *ps* timescale [35–39]. Following ground state chromophore relaxation and minor side chain readjustments, a spectrally P_r-like intermediate termed Meta-F is formed on the *ps*-to-*ns* timescale [36, 40, 41]. The Meta-F intermediate undergoes rearrangement of the hydrogen-bonding network and the

binding pocket, as well as refolding of the tongue to form the P_r state [41]. These steps occur on the *μs-ms* timescale and do not involve major spectral changes in the visible spectral range [40, 42, 43].

In this work, we expand our ultrafast studies on knotless phytochromes [18, 19] to the *ms* timescale. We compare the *ms* dynamics of the knotless phytochrome All2699g1g2 and its isolated GAF domain All2699g1 to reveal the effect of the PHY-like g2 domain on the forward ($P_r \rightarrow P_{fr}$) and reverse ($P_{fr} \rightarrow P_r$) photoconversion of knotless phytochromes. We further compare our results to the previously investigated knotless phytochrome *Syn*Cph2 and discuss the similarities and differences observed for these structurally related knotless phytochromes.

2 Materials and methods

2.1 Protein preparation

Preparation of All2699g1 and All2699g1g2 was described elsewhere in detail [19, 44]. The final buffer conditions for the experiments were set to 50 mM TRIS, 200 mM NaCl, 5% Glycerol, pH 8.0. For the pH dependence measurements of All2699g1, the following buffer conditions were used: 20 mM MES, 150 mM NaCl, 5% Glycerol, pH 6.1; 20 mM KPB, 150 mM NaCl, 5% Glycerol, pH 7.2; 20 mM TRIS, 150 mM NaCl, 5% Glycerol, pH 8.4.

Preparation of *Syn*Cph2 was described elsewhere [9]. The final buffer conditions for the experiments were set to 50 mM TRIS, 300 mM NaCl, 5 mM EDTA, pH 8.0.

Samples were measured in a 2×10 mm quartz cuvette with an optical density between 0.4 and 0.8 on 10 mm.

2.2 Stationary characterization

Stationary absorption spectra of the investigated samples were obtained using a Specord S600 absorption spectrometer (Analytik Jena). Conversion between the P_r and the P_{fr} state was achieved by illumination with appropriate LEDs (730 nm and 590 nm respectively, 1 W, Thorlabs).

2.3 Transient flash photolysis experiments

The pump pulses were provided by an optical parametric oscillator (OPO) (preciScan, GWU-Lasertechnik) pumped by a Nd:YAG laser (SpitLight 600, Innolas Laser). The OPO was set to 640 nm for P_r and 702 nm for P_{fr} measurements with an average pulse energy of 2.4–2.6 mJ/cm². The probe light was generated by a spectrally broad continuous wave Xenon lamp (Hamamatsu LC-8) and two matched monochromators before and after the sample. The absorbance changes were then detected with a photomultiplier tube

(PMT) and the resulting signal was converted into an electrical signal and recorded using an oscilloscope (DPO5204B-10RL, Tektronix). Time points were measured every 100 ns, except for the g1g2 P_{fr} measurements where a point was measured every 200 ns. For all samples absorbance changes were recorded between 500 and 750 nm with at least 30 averaged scans per wavelength. Between each individual scan the sample was illuminated for 4 s using an appropriate LED ($P_r \rightarrow P_{fr}$, 730 nm; $P_{fr} \rightarrow P_r$, 590 nm) to avoid accumulation of photoproducts. For analysis, the single transients were reduced by averaging data points in a combined linear and logarithmic timescale to obtain feasible data sizes.

For the pH dependence measurements of the *ms* dynamics of All2699g1, transients at six key wavelengths (510, 540, 600, 630, 680, and 710 nm) were measured and analyzed like the complete datasets. To validate the reduction to the 6-wavelength datasets, a comparison of the analysis to a complete dataset is shown exemplarily in the SI for pH 7.2 (SI Fig. S1).

2.4 Data analysis

Data analysis was performed using OPTIMUS (http://www.optimusfit.org/) [45]. We performed global target analysis (GTA) [45, 46] on all datasets using a sequential model. This model is fitted directly to the experimental data and results in the lifetimes, the decay-associated spectra (DAS) and the so-called evolution-associated difference spectra (EADS) for the respective kinetic components. The DAS contain both spectral and kinetic information, i.e. the positive amplitudes in the DAS account for decay of photoproduct absorption (PA) while negative amplitudes account for rise of absorption or recovery of the ground state bleach. Unlike DAS, EADS contain pure spectral information.

3 Results and discussion

3.1 Forward ($P_r \rightarrow P_{fr}$) *ms* dynamics

3.1.1 Comparison between All2699g1 and All2699g1g2

The flash photolysis data of the P_r state of All2699g1 and All2699g1g2 (Fig. 2) appear very similar. Both show a dominant negative difference signal visible throughout the entire detected time range, which can be straightforwardly assigned to the ground state bleach (GSB) of the P_r state after excitation. Additionally, several distinct positive signals, at 660–690 nm, 660–700 nm, 500–560 nm and 660–750 nm, are present at different delay times in the data. These absorption changes are associated with the different intermediates observed during the photocycle. We performed global target
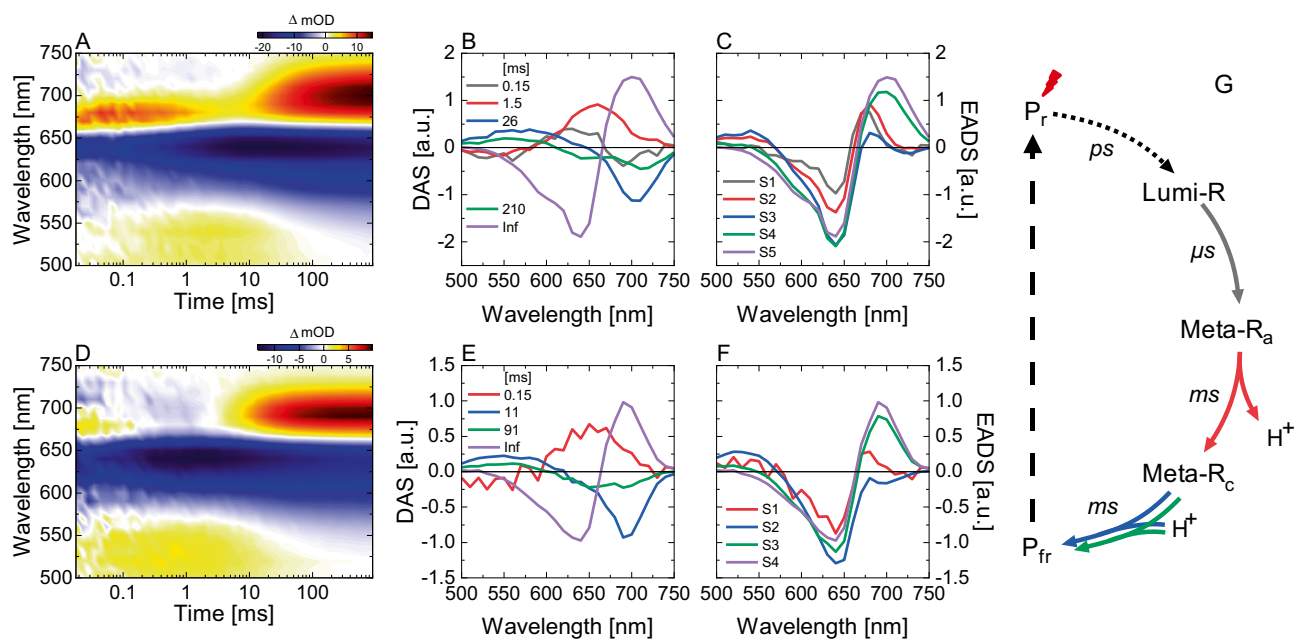
Fig. 2 $P_r \rightarrow P_{fr}$ *ms* dynamics of All2699g1g2 (**A**–**C**) and All2699g1 (**D**–**F**) at pH 8. **A**, **D** Flash photolysis data of the $P_r \rightarrow P_{fr}$ *ms* dynamics after excitation at 640 nm. **B**, **E** Corresponding decay-associated spectra (DAS) and **C**, **F** evolution-associated spectra (EADS) obtained after global target analysis of (A,D). **G** Schematic repre-

sentation of the proposed photocycle for the $P_r \rightarrow P_{fr}$ *ms* dynamics of All2699g1g2 and All2699g1 at pH 8. The dashed line indicates the thermal reversion from P_{fr} to P_r, while the dotted line represents the initial photoreaction

analysis using a sequential model to reveal the kinetic details of the $P_r \rightarrow P_{fr}$ conversion.

Five components were required to fit the P_r data of All2699g1g2. Based on the resemblance to the primary photoproduct formed on the ultrafast timescale [18], we assign the S1 evolution-associated difference spectrum (EADS, Fig. 2C), peaking at 675 nm, to the Lumi-R intermediate. The positive (575–660 nm) and negative amplitudes (660–730 nm) of the 150 μs decay-associated spectrum (DAS, Fig. 2B), indicate the Lumi-R-to-Meta-R_a transition, which occurs with a red spectral shift (S1 vs. S2 EADS) induced by the bilin chromophore relaxation. In a next step, the chromophore undergoes a prominent spectral blue shift with a 1.5 ms lifetime to form the Meta-R_c intermediate (positive amplitude DAS at 575–750 nm and negative amplitude DAS at 500–575 nm in Fig. 2B, S2 → S3 EADS transition in Fig. 2C). We attribute this blue spectral shift to a chromophore deprotonation step following the assignment made previously for other phytochromes [31, 33, 34]. The following re-protonation of the chromophore is biphasic (S3 and S4 EADS). The corresponding DAS show similar spectral features representing the decay of the Meta-R_c absorption (positive amplitude at about 550 nm in τ_3 (26 ms) and in τ_4 (210 ms)) and the rise of the absorption of the final photoproduct P_{fr} (negative amplitude 650–750 nm). In contrast to τ_3, the DAS amplitude of τ_4 is negative in the range of 610–650 nm, potentially indicating some recovery of the

spectrally coinciding P_r ground state via a shunt pathway as reported in some bacteriophytochromes [47, 48].

The major difference between the P_r flash photolysis data of All2699g1g2 (Fig. 2A) and All2699g1 (Fig. 2D) is that for g1 the kinetics is accelerated and can be described with only four components (Fig. 2E-F). Following the assignment above, those four components correspond to Meta-R_a (660–700 nm), Meta-R_c (500–560 nm), P_{fr} (660–740 nm) and the P_r GSB. The Lumi-R-to-Meta-R_a transition occurs on a timescale shorter than what is detected in our experiment (i.e. < 20 μs). Thus, the 150 μs component represents instead the Meta-R_a-to-Meta-R_c transition as indicated by the negative amplitude between 500 and 550 nm in the corresponding DAS (Fig. 2E). The Meta-R_c decay in All2699g1, albeit accelerated, is also biphasic (11 ms and 91 ms lifetimes, see below for more detailed discussion).

3.1.2 Effect of the PHY domain on the forward dynamics

The Lumi-R-to-Meta-R_a and Meta-R_a-to-Meta-R_c transitions are significantly slower (~ 10-fold) in All2699g1g2 as compared to All2699g1, which indicates that the presence of the PHY domain imposes a higher energetic barrier for the associated chromophore relaxation and proximal protein structural rearrangements. This conclusion is in line with previous NMR [23, 49] and RR [28] studies, where it was proposed that the interaction with the PHY tongue makes

the chromophore-binding pocket more rigid. In contrast, the final chromophore transition (Meta-R_c-to-P_{fr}), typically associated with major structural changes (tongue refolding [20, 21, 24, 32]) in the protein environment distal to the chromophore, is affected to a smaller extent (twofold) by the lacking PHY domain in All2699g1. Furthermore, the preserved biphasic character of the Meta-R_c-to-P_{fr} transition in All2699g1 suggests that the chromophore transitions associated with this step are predominantly determined by factors within the binding pocket of the GAF domain. Previously, a similar conclusion was derived based on time-resolved X-ray and UV/Vis studies on *Dr*BphP [21].

3.1.3 Origin of the biphasic meta-R_c to P_{fr} transition

To further investigate the origin of the biphasic Meta-R_c-to-P_{fr} kinetics in All2699g1 and All2699g1g2, we performed flash photolysis measurements at selected detection wavelengths (510, 540, 600, 630, 680, and 710 nm) and at three different pH values (6.1, 7.2, and 8.4). A direct comparison of the transients at 710 nm reveals that the P_{fr} formation is significantly accelerated at high pH values (Fig. 3A). This clear pH dependence is further corroborated by the DAS of the three datasets (Fig. 3B).

While the lifetime components do not vary significantly, their corresponding amplitudes and especially the amplitude ratio between the shorter and the longer component (correspondingly marked blue and green in Fig. 3B) change with the pH. At pH 6.1, the amplitude of the longer component is higher than that of the shorter one resulting in the slowest overall Meta-R_c-to-P_{fr} transition (Fig. 3A). At pH 8.4 the ratio is reversed, the shorter component clearly dominates, thus making the overall Meta-R_c decay fastest. At pH 7.2 the two components have nearly identical amplitude. Consequently, the process occurring with the shorter lifetime component is favored at high pH, while the process described by the longer lifetime component is favored at low pH. Furthermore, the monoexponential formation of the Meta-R_c and the lack of spectral differences in the two DAS describing

its decay imply that there is a single chromophore population in Meta-R_c and that the following re-protonation reaction is dependent on the pKa value of the proton donor residue and the state of the hydrogen-bonding network linking it to the solvent. Thereby, the faster component represents a chromophore re-protonation reaction occurring from a protonated residue, while for the slower component the residue is deprotonated, and thus the re-protonation requires proton uptake from the environment. Such a proton uptake step has been reported for Cph1 [30]. In effect, the role of the slower component is prominent at low pH, while at higher (H^+ deficient) pH, its contribution is diminished.

While we cannot directly identify the relevant residue, based on the nearly identical amplitudes of the DAS of the two Meta-R_c decay components, we can deduce that its pKa value is close to 7.2. Mutational studies on other phytochromes (*Syn*Cph1, *Dr*BphP, Agp1) identified histidine residues that are part of the extended hydrogen-bonding network of the chromophore and affect its protonation state [33, 50–53]. The respective residues in All2699g1, His139 and His169, are therefore potential candidates for the origin of the observed pH dependence. His139 is in direct contact with the pyrrole nitrogens of the bilin chromophore and was reported to be directly involved in the proton uptake leading to the formation of the P_{fr} state as some mutants of this residue do not progress past Meta-R_c in their photocycle [33, 52]. In addition, the His139-homologous residue H260 exhibits a pKa value of 7.4 in the P_r state of *Syn*Cph1, strikingly similar to the value we derive here for the biphasic transition to P_{fr} [51]. His169 is part of the extended hydrogen-bonding network, and thus it is in an indirect contact with His139. It is also in contact with the chromophore in both P_r and P_{fr} interacting with the D-ring carbonyl or the C-ring propionate, respectively [54]. As such, its protonation state could influence the hydrogen-bonding network potentially contributing to the biphasic kinetics. However, we consider His139 a more likely candidate since mutants of His169 exhibit only minor impact on the chromophore and/or hydrogen-bonding network pKa [50]. The highly
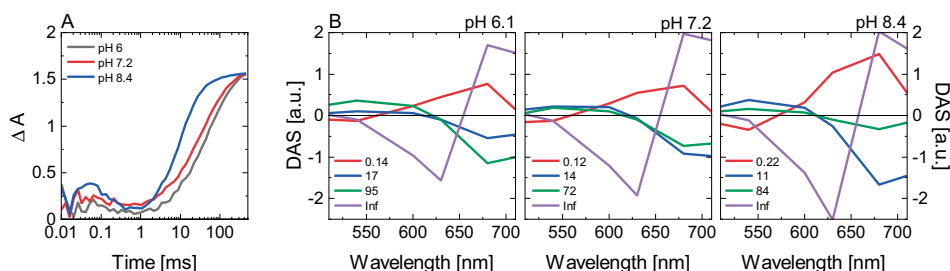
Fig. 3 pH dependence of the $P_r \rightarrow P_{fr}$ *ms* dynamics of All2699g1 at pH 6.1, 7.2 and 8.4. **A** Transients of the UV/Vis flash photolysis measurements of All2699g1 at 710 nm at different pH values. **B** DAS obtained by global lifetime analysis of 6 transients at key wavelengths (510, 540, 600, 630, 680 and 710 nm) of All2699g1 after excitation at 640 nm at different pH values

conserved Asp87 may also be considered as a candidate involved in the protonation steps. This residue interacts with the chromophore through the pyrrole water and similar to His139 is involved in tuning the chromophore pKa and its hydrogen-bonding network [33, 52]. However, it is reported that this Asp87 retains its protonation state during the photocycle rendering a direct involvement in the reprotonation unlikely [24]. Indirectly, an increase in the protein mobility, such as that observed in *Syn*Cph1 [34], may also be contributing to the overall acceleration of P_{fr} formation at higher pH.

3.1.4 Comparison of the P_r dynamics to other phytochromes

The lifetimes of the intermediates observed in the knotless phytochrome All2699g1g2 match well with previously reported lifetimes for *Syn*Cph1 [30], *Syn*Cph2 [32], and Agp1 [31] indicating high similarities between the dynamics of knotless and knotted phytochromes on the *ms* timescale. In the only investigated knotless phytochrome *Syn*Cph2, the lifetimes for the Lumi-R-to-Meta-R_a and Meta-R_a-to-Meta-R_c transition (170 μs and 1.6 ms, SI Fig. S2) are nearly identical to those found here for All2699g1g2 (150 μs and 1.5 ms, Fig. 2B). However, the Meta-R_c-to-P_{fr} transition is significantly faster in *Syn*Cph2 and proceeds monoexponentially with a lifetime of 17 ms. In contrast, the

Meta-R_c-to-P_{fr} transition in *Syn*Cph1 is similarly biphasic with lifetimes close to those we find in All2699g1g2. A comparison between *Syn*Cph2 and All2699g1 shows a different involvement of water molecules and propionic side chains in the extended hydrogen-bonding network, which can result in different pKa values and explain the occurrence or lack of biphasic Meta-R_c decay in different phytochromes.

3.2 Reverse ($P_{fr} \rightarrow P_r$) *ms* dynamics

3.2.1 Comparison of All2699g1 and All2699g1g2

To provide a complete picture of the influence of the PHY domain on the dynamics of knotless phytochromes, we investigated the *ms* reverse reaction ($P_{fr} \rightarrow P_r$) in All2699g1 and All2699g1g2. The GSB (negative absorption difference) signal in the P_{fr} flash photolysis data of both samples is located above 650 nm (Fig. 4). However, reflecting the difference in the P_{fr} absorption spectra (Fig. 1), the GSB of All2699g1g2 is red shifted. In addition to the GSB signal, we observe a spectral evolution of the positive absorption difference signal associated with the transitions of the intermediate states towards the final photoproduct P_r (*i.e.* from ~550–650 nm through ~575–660 nm to ~500–630 nm, Fig. 1). This evolution is better discerned for All2699g1g2.

The global target analysis with a sequential scheme yields four lifetime components for both samples. In All2699g1g2,
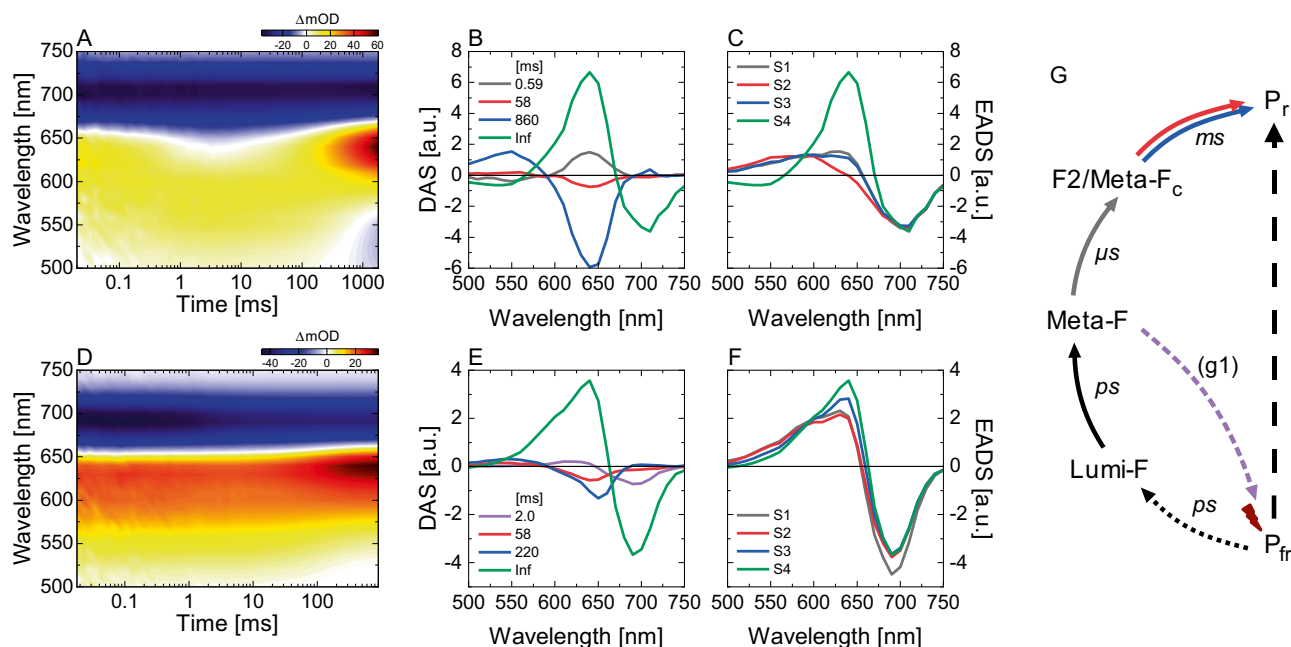
Fig. 4 $P_{fr} \rightarrow P_r$ *ms* dynamics of All2699g1g2 (**A–C**) and All2699g1 (**D–F**) at pH 8. **A, D** Flash photolysis data of the $P_{fr} \rightarrow P_r$ *ms* dynamics after excitation at 702 nm. (B,E) Corresponding decay-associated spectra (DAS) and **C, F** evolution-associated spectra (EADS) obtained after global target analysis of **A, D**. **G** Schematic represen-

tation of the proposed photocycle for the $P_{fr} \rightarrow P_r$ *ms* dynamics of All2699g1g2 and All2699g1 at pH 8. The vertical black dashed line indicates the thermal reversion from P_{fr} to P_r, while the dotted line represents the initial photoreaction. The short dashed purple line represents the shunt pathway present in All2699g1

the S1 EADS (Fig. 4C) resembles the spectrum of the species present at the end of the ultrafast P_{fr} dynamics in *Syn*Cph2 [37] or *Syn*Cph1 [36], and thus can be assigned to the Meta-F intermediate. Meta-F decays with a lifetime of 590 μs to form a blue-shifted intermediate (S2 EADS) as described by the positive–negative amplitudes of the corresponding DAS (Fig. 4B). A similar blue-shifted species has also been observed in *Syn*Cph2 and termed F2 [32]. The F2 intermediate then decays to form the final P_r state with two lifetimes where the amplitude of the 860 ms component is significantly higher than that of the 58 ms component (Fig. 4B).

The P_{fr} flash photolysis data of All2699g1 exhibit similar signals (Fig. 4D). However, the S1 EADS is broadened on the blue spectral side, which indicates that the F2 intermediate is already present at the beginning of the measurement in equilibrium with Meta-F (Fig. 4F). Thus, in analogy to Meta-R_a from the forward dynamics of All2699g1, in the reverse direction we cannot clearly detect the rise of F2 in the single domain sample. Instead, the first lifetime component (2 ms) in All2699g1 indicates a shunt pathway to the P_{fr} ground state from a leftover Meta-F population. Such a pathway is not present in the reverse dynamics of All2699g1g2 and is not observed in *Syn*Cph2, but has been observed in bacteriophytochromes [47, 48]. The following transition from F2 to the P_r state is described again by two lifetimes. However, in contrast to All2699g1g2, the difference in the amplitude of the two components is much smaller. In addition, the second lifetime component is significantly shorter in All2699g1 (i.e. 220 ms). As a result, the overall P_r formation is accelerated in All2699g1. Interestingly, in both samples, there appears to be an equilibrium between the Meta-F and F2 intermediates. This equilibrium is shifted towards Meta-F in All2699g1, while in All2699g1g2 the F2 and Meta-F intermediates have similar amplitudes. The S3 EADS of All2699g1g2 (Fig. 4C) suggests that at longer timescales the equilibrium shifts towards high F2 populations.

3.2.2 Effect of the PHY domain on the reverse dynamics

In both the forward and the reverse dynamics, the photoreaction is accelerated in absence of the PHY domain, i.e. the Meta-R_a in the forward and F2 in the reverse dynamics are formed in All2699g1 earlier than in All2699g1g2. We attribute this to fewer restrictions in the binding pocket in absence of the PHY domain as revealed by previous NMR and cryo-trapping experiments [23, 28, 49]. The photoreaction then follows similar steps where an intermediate spectrally close to the final photoproduct (Meta-R_a and Meta-F) converts into a blue-shifted one (Meta-R_c and F2). The final photoproduct (P_{fr} or P_r) is formed with a biphasic kinetics, as indicated by a corresponding red shift on the *ms* timescale. Similar to the spectral shift of Meta-R_c in the forward direction, we

observe a spectral shift of F2 in the reverse direction. This resemblance suggests that the formation and the decay of F2 may also occur via deprotonation and re-protonation steps. For consistency, we propose that F2 is termed Meta-F_c by analogy to Meta-R_c.

3.2.3 Comparison of the P_{fr} dynamics to other phytochromes

It is particularly remarkable that the Meta-F-to-Meta-F_c transition in All2699g1g2 is on a timescale (hundreds of μs) similar to that found in *Syn*Cph2 and PhyA while the P_r formation step is two orders of magnitude slower [32, 40]. Even in comparison to other phytochromes like CphA [40] or *Pst*BphP1 and *Pa*BphP1 [43] that exhibit slightly different reverse kinetics, the formation of the photoproduct is still exceptionally slow in both All2699g1g2 and All2699g1. The unknown origin of the striking temporal difference for the final photoproduct formation step between the two structurally very similar knotless phytochromes (All2699g1g2 and *Syn*Cph2) should be addressed in future studies.

4 Conclusion

Our work provides a dynamic picture of the effect of the PHY domain on the *ms* dynamics of knotless phytochromes. We show that the occurrence and spectral signature of the involved intermediates are not significantly affected by the presence of the PHY domain. However, the *μs* dynamics involving relaxation of the chromophore are slowed down for both the forward and the reverse direction. We attribute this effect to a more confined chromophore binding pocket in presence of the PHY domain. Quite remarkably, the lifetimes describing the transition to the final photoproduct are much less affected by the presence/absence of the PHY domain. This supports previous findings that the rate limiting step of the photoproduct formation observed by UV/vis spectroscopy is imposed by internal factors of the GAF (PAS-GAF) domain and are not directly related to tongue refolding.

Interestingly, we find that the Meta-R_c-to-P_{fr} transition is biphasic in both All2699g1 and All2699g1g2, but not in *Syn*Cph2. Based on the pH dependence of the transition in All2699g1, we associate this behavior to the pKa value of the proton donor residue in the Meta-R_c intermediate. The lack of biphasic behavior in some phytochromes suggests that the rate of photoproduct formation can be tweaked through fine tuning of the pKa value of the hydrogen-bonding network.

Declarations

Conflict of interest The datasets generated during and/or analyzed during the current study are available from the corresponding author upon reasonable request. The authors have no competing interests to declare that are relevant to the content of this article.

References

1. Anders, K., & Essen, L. O. (2015). The family of phytochrome-like photoreceptors: Diverse, complex and multi-colored, but very useful. *Current Opinion in Structural Biology, 35*, 7–16. https://doi.org/10.1016/j.sbi.2015.07.005

2. Rockwell, N. C., & Lagarias, J. C. (2017). Phytochrome diversification in cyanobacteria and eukaryotic algae. *Current Opinion in Plant Biology, 37*, 87–93. https://doi.org/10.1016/j.pbi.2017.04.003

3. Rockwell, N. C., & Lagarias, J. C. (2006). The structure of phytochrome: A picture is worth a thousand spectra. *The Plant Cell, 18*(1), 4–14. https://doi.org/10.1105/tpc.105.038513

4. Rockwell, N. C., Su, Y.-S., & Lagarias, J. C. (2006). Phytochrome structure and signaling mechanisms. *Annual Review of Plant Biology, 57*(1), 837–858. https://doi.org/10.1146/annurev.arplant.56.032604.144208

5. Möglich, A., Yang, X., Ayers, R. A., & Moffat, K. (2010). Structure and function of plant photoreceptors. *Annual Review of Plant Biology, 61*, 21–47. https://doi.org/10.1146/annurev-arplant-042809-112259

6. Yang, X., Kuk, J., & Moffat, K. (2008). Crystal structure of Pseudomonas aeruginosa bacteriophytochrome: Photoconversion and signal transduction. *Proceedings of the National Academy of Sciences of the United States of America, 105*(38), 14715–14720. https://doi.org/10.1073/pnas.0806718105

7. Essen, L. O., Mailliet, J., & Hughes, J. (2008). The structure of a complete phytochrome sensory module in the Pr ground state. *Proceedings of the National Academy of Sciences of the United States of America, 105*(38), 14709–14714. https://doi.org/10.1073/pnas.0806477105

8. Ikeuchi, M., & Ishizuka, T. (2008). Cyanobacteriochromes: A new superfamily of tetrapyrrole-binding photoreceptors in cyanobacteria. *Photochemical and Photobiological Sciences, 7*(10), 1159. https://doi.org/10.1039/b802660m

9. Anders, K., Von Stetten, D., Mailliet, J., Kiontke, S., Sineshchekov, V. A., Hildebrandt, P., Hughes, J., & Essen, L. O. (2011). Spectroscopic and photochemical characterization of the red-light sensitive photosensory module of Cph2 from synechocystis PCC 6803. *Photochemistry and Photobiology, 87*(1), 160–173. https://doi.org/10.1111/j.1751-1097.2010.00845.x

10. Lamparter, T., Mittmann, F., Gartner, W., Borner, T., Hartmann, E., & Hughes, J. (1997). Characterization of recombinant phytochrome from the cyanobacterium Synechocystis. *Proceedings of the National Academy of Sciences, 94*(22), 11792–11797. https://doi.org/10.1073/pnas.94.22.11792

11. Lamparter, T., Michael, N., Mittmann, F., & Esteban, B. (2002). Phytochrome from Agrobacterium tumefaciens has unusual spectral properties and reveals an N-terminal chromophore attachment site. *Proceedings of the National Academy of Sciences, 99*(18), 11628–11633. https://doi.org/10.1073/pnas.152263999

12. Chai, Y. G., Singh, B. R., Song, P. S., Lee, J., & Robinson, G. W. (1987). Purification and spectroscopic properties of 124-kDa oat phytochrome. *Analytical Biochemistry, 163*(2), 322–330. https://doi.org/10.1016/0003-2697(87)90231-4

13. Hirose, Y., Shimada, T., Narikawa, R., Katayama, M., & Ikeuchi, M. (2008). Cyanobacteriochrome CcaS is the green light receptor that induces the expression of phycobilisome linker protein. *Proceedings of the National Academy of Sciences, 105*(28), 9528–9533. https://doi.org/10.1073/pnas.0801826105

14. Rockwell, N. C., Martin, S. S., Gulevich, A. G., & Lagarias, J. C. (2012). Phycoviolobilin formation and spectral tuning in the DXCF cyanobacteriochrome subfamily. *Biochemistry, 51*(7), 1449–1463. https://doi.org/10.1021/bi201783j

15. Rockwell, N. C., Martin, S. S., Feoktistova, K., & Lagarias, J. C. (2011). Diverse two-cysteine photocycles in phytochromes and cyanobacteriochromes. *Proceedings of the National Academy of Sciences of the United States of America, 108*(29), 11854–11859. https://doi.org/10.1073/pnas.1107844108

16. Rockwell, N. C., Martin, S. S., & Lagarias, J. C. (2016). Identification of Cyanobacteriochromes detecting far-red light. *Biochemistry, 55*(28), 3907–3919. https://doi.org/10.1021/acs.biochem.6b00299

17. Fushimi, K., Ikeuchi, M., & Narikawa, R. (2017). The expanded red/green Cyanobacteriochrome lineage: An evolutionary hot spot. *Photochemistry and Photobiology, 93*(3), 903–906. https://doi.org/10.1111/php.12764

18. Fischer, T., Xu, Q.-Z., Zhao, K.-H., Gärtner, W., Slavov, C., & Wachtveitl, J. (2020). Effect of the PHY domain on the photoisomerization step of the forward Pr→Pfr conversion of a knotless phytochrome. *Chemistry A European Journal*. https://doi.org/10.1002/chem.202003138

19. Slavov, C., Fischer, T., Barnoy, A., Shin, H., Rao, A. G., Wiebeler, C., Zeng, X., Sun, Y., Xu, Q., Gutt, A., Zhao, K., Gärtner, W., Yang, X., Schapiro, I., & Wachtveitl, J. (2020). The interplay between chromophore and protein determines the extended excited state dynamics in a single-domain phytochrome. *Proceedings of the National Academy of Sciences of the United States of America, 117*(28), 16356–16362. https://doi.org/10.1073/pnas.1921706117

20. Takala, H., Björling, A., Berntsson, O., Lehtivuori, H., Niebling, S., Hoernke, M., Kosheleva, I., Henning, R., Menzel, A., Ihalainen, J. A., & Westenhoff, S. (2014). Signal amplification and transduction in phytochrome photosensors. *Nature, 509*(7499), 245–248. https://doi.org/10.1038/nature13310

21. Björling, A., Berntsson, O., Lehtivuori, H., Takala, H., Hughes, A. J., Panman, M., Hoernke, M., Niebling, S., Henry, L., Henning,

R., Kosheleva, I., Chukharev, V., Tkachenko, N. V., Menzel, A., Newby, G., Khakhulin, D., Wulff, M., Ihalainen, J. A., & Westenhoff, S. (2016). Structural photoactivation of a full-length bacterial phytochrome. *Science Advances, 2*(8), e1600920. https://doi.org/10.1126/sciadv.1600920

22. Anders, K., Daminelli-Widany, G., Mroginski, M. A., Von Stetten, D., & Essen, L. O. (2013). Structure of the cyanobacterial phytochrome 2 photosensor implies a tryptophan switch for phytochrome signaling. *Journal of Biological Chemistry, 288*(50), 35714–35725. https://doi.org/10.1074/jbc.M113.510461

23. Xu, Q.-Z., Bielytskyi, P., Otis, J., Lang, C., Hughes, J., Zhao, K.-H., Losi, A., Gärtner, W., & Song, C. (2019). MAS NMR on a red/far-red photochromic Cyanobacteriochrome All2699 from Nostoc. *International Journal of Molecular Sciences, 20*(15), 3656. https://doi.org/10.3390/ijms20153656

24. Ihalainen, J. A., Gustavsson, E., Schroeder, L., Donnini, S., Lehtivuori, H., Isaksson, L., Thöing, C., Modi, V., Berntsson, O., Stucki-Buchli, B., Liukkonen, A., Häkkänen, H., Kalenius, E., Westenhoff, S., & Kottke, T. (2018). Chromophore-protein interplay during the phytochrome photocycle revealed by step-scan FTIR spectroscopy. *Journal of the American Chemical Society, 140*(39), 12396–12404. https://doi.org/10.1021/jacs.8b04659

25. Braslavsky, S. E., Gärtner, W., & Schaffner, K. (1997). Phytochrome photoconversion. *Plant, Cell and Environment, 20*(6), 700–706. https://doi.org/10.1046/j.1365-3040.1997.d01-101.x

26. Schmidt, P., Westphal, U. H., Worm, K., Braslavsky, S. E., Gärtner, W., & Schaffner, K. (1996). Chromophore-protein interaction controls the complexity of the phytochrome photocycle. *Journal of Photochemistry and Photobiology B, 34*(1), 73–77. https://doi.org/10.1016/1011-1344(95)07269-1

27. Zhang, C. F., Farrens, D. L., Björling, S. C., Song, P. S., & Kliger, D. S. (1992). Time-resolved absorption studies of native etiolated oat phytochrome. *Journal of the American Chemical Society, 114*(12), 4569–4580. https://doi.org/10.1021/ja00038a019

28. Velazquez Escobar, F., Kneip, C., Michael, N., Hildebrandt, T., Tavraz, N., Gärtner, W., Hughes, J., Friedrich, T., Scheerer, P., Mroginski, M. A., & Hildebrandt, P. (2020). The lumi-R intermediates of prototypical phytochromes. *Journal of Physical Chemistry B, 124*(20), 4044–4055. https://doi.org/10.1021/acs.jpcb.0c01059

29. Kübel, J., Chenchiliyan, M., Ooi, S. A., Gustavsson, E., Isaksson, L., Kuznetsova, V., Ihalainen, J. A., Westenhoff, S., & Maj, M. (2020). Transient IR spectroscopy identifies key interactions and unravels new intermediates in the photocycle of a bacterial phytochrome. *Physical Chemistry Chemical Physics, 22*(17), 9195–9203. https://doi.org/10.1039/c9cp06995j

30. Van Thor, J. J., Borucki, B., Crielaard, W., Otto, H., Lamparter, T., Hughes, J., Hellingwerf, K. J., & Heyn, M. P. (2001). Light-induced proton release and proton uptake reactions in the cyanobacterial phytochrome Cph1. *Biochemistry, 40*(38), 11460–11471. https://doi.org/10.1021/bi002651d

31. Borucki, B., von Stetten, D., Seibeck, S., Lamparter, T., Michael, N., Mroginski, M. A., Otto, H., Murgida, D. H., Heyn, M. P., & Hildebrandt, P. (2005). Light-induced proton release of phytochrome is coupled to the transient deprotonation of the tetrapyrrole chromophore. *Journal of Biological Chemistry, 280*(40), 34358–34364. https://doi.org/10.1074/jbc.M505493200

32. Anders, K., Gutt, A., Gärtner, W., & Essen, L. O. (2014). Phototransformation of the red light sensor cyanobacterial phytochrome 2 from synechocystis species depends on its tongue motifs. *Journal of Biological Chemistry, 289*(37), 25590–25600. https://doi.org/10.1074/jbc.M114.562082

33. Von Stetten, D., Seibeck, S., Michael, N., Scheerer, P., Mroginski, M. A., Murgida, D. H., Krauss, N., Heyn, M. P., Hildebrandt, P., Borucki, B., & Lamparter, T. (2007). Highly conserved residues Asp-197 and His-250 in Agp1 phytochrome control the proton affinity of the chromophore and Pfr formation. *Journal of Biological Chemistry, 282*(3), 2116–2123. https://doi.org/10.1074/jbc.M608878200

34. Sadeghi, M., Balke, J., Schneider, C., Nagano, S., Stellmacher, J., Lochnit, G., Lang, C., Weise, C., Hughes, J., & Alexiev, U. (2020). Transient deprotonation of the chromophore affects protein dynamics proximal and distal to the linear tetrapyrrole chromophore in phytochrome Cph1. *Biochemistry, 59*(9), 1051–1062. https://doi.org/10.1021/acs.biochem.9b00967

35. Heyne, K., Herbst, J., Stehlik, D., Esteban, B., Lamparter, T., Hughes, J., & Diller, R. (2002). Ultrafast dynamics of phytochrome from the cyanobacterium Synechocystis, reconstituted with phycocyanobilin and phycoerythrobilin. *Biophysical Journal, 82*(2), 1004–1016. https://doi.org/10.1016/S0006-3495(02)75460-X

36. Kim, P. W., Rockwell, N. C., Martin, S. S., Lagarias, J. C., & Larsen, D. S. (2014). Heterogeneous photodynamics of the Pfr state in the cyanobacterial phytochrome Cph1. *Biochemistry, 53*(28), 4601–4611. https://doi.org/10.1021/bi5005359

37. Fischer, T., van Wilderen, L. J. G. W., Gnau, P., Bredenbeck, J., Essen, L.-O., Wachtveitl, J., & Slavov, C. (2021). Ultrafast photoconversion dynamics of the knotless phytochrome SynCph2. *International Journal of Molecular Sciences, 22*(19), 10690. https://doi.org/10.3390/ijms221910690

38. Rohmer, T., Lang, C., Bongards, C., Gupta, K. B. S. S., Neugebauer, J., Hughes, J., Gärtner, W., & Matysik, J. (2010). Phytochrome as molecular machine: Revealing chromophore action during the Pfr → Pr photoconversion by magic-angle spinning NMR spectroscopy. *Journal of the American Chemical Society, 132*(12), 4431–4437. https://doi.org/10.1021/ja9108616

39. Yang, X., Ren, Z., Kuk, J., & Moffat, K. (2011). Temperature-scan cryocrystallography reveals reaction intermediates in bacteriophytochrome. *Nature, 479*(7373), 428–431. https://doi.org/10.1038/nature10506

40. Chizhov, I., Zorn, B., Manstein, D. J., & Gärtner, W. (2013). Kinetic and thermodynamic analysis of the light-induced processes in plant and cyanobacterial phytochromes. *Biophysical Journal, 105*(9), 2210–2220. https://doi.org/10.1016/j.bpj.2013.09.033

41. Kraskov, A., Nguyen, A. D., Goerling, J., Buhrke, D., Velazquez Escobar, F., Fernandez Lopez, M., Michael, N., Sauthof, L., Schmidt, A., Piwowarski, P., Yang, Y., Stensitzki, T., Adam, S., Bartl, F., Schapiro, I., Heyne, K., Siebert, F., Scheerer, P., Mroginski, M. A., & Hildebrandt, P. (2020). Intramolecular proton transfer controls protein structural changes in phytochrome. *Biochemistry, 59*(9), 1023–1037. https://doi.org/10.1021/acs.biochem.0c00053

42. Chen, E., Lapko, V. N., Lewis, J. W., Song, P. S., & Kliger, D. S. (1996). Mechanism of native oat phytochrome photoreversion: A time-resolved absorption investigation. *Biochemistry, 35*(3), 843–850. https://doi.org/10.1021/bi952115z

43. Consiglieri, E., Gutt, A., Gärtner, W., Schubert, L., Viappiani, C., Abbruzzetti, S., & Losi, A. (2019). Dynamics and efficiency of photoswitching in biliverdin-binding phytochromes. *Photochemical and Photobiological Sciences, 18*(10), 2484–2496. https://doi.org/10.1039/c9pp00264b

44. Xu, Q.-Z., Goett-Zink, L., Gärtner, W., Zhao, K.-H., & Kottke, T. (2020). Tongue refolding in the knotless Cyanobacterial phytochrome All2699. *Biochemistry, 59*(22), 2047–2054. https://doi.org/10.1021/acs.biochem.0c00209

45. Slavov, C., Hartmann, H., & Wachtveitl, J. (2015). Implementation and evaluation of data analysis strategies for time-resolved optical spectroscopy. *Analytical Chemistry, 87*(4), 2328–2336. https://doi.org/10.1021/ac504348h

46. Van Stokkum, I. H. M. M., Larsen, D. S., & van Grondelle, R. (2004). Global and target analysis of time-resolved spectra.

Biochimica et Biophysica Acta, 1657(2–3), 82–104. https://doi.org/10.1016/j.bbabio.2004.04.011

47. Merga, G., Lopez, M. F., Fischer, P., Piwowarski, P., Nogacz, Ż, Kraskov, A., Buhrke, D., Escobar, F. V., Michael, N., Siebert, F., Scheerer, P., Bartl, F., & Hildebrandt, P. (2021). Light-and temperature-dependent dynamics of chromophore and protein structural changes in bathy phytochrome Agp2. *Physical Chemistry Chemical Physics, 23*(33), 18197–18205. https://doi.org/10.1039/d1cp02494a

48. Buhrke, D., Kuhlmann, U., Michael, N., & Hildebrandt, P. (2018). The photoconversion of phytochrome includes an unproductive shunt reaction pathway. *ChemPhysChem, 19*(5), 566–570. https://doi.org/10.1002/cphc.201701311

49. Kim, Y., Xu, Q.-Z., Zhao, K.-H., Gärtner, W., Matysik, J., & Song, C. (2020). Lyophilization reveals a multitude of structural conformations in the chromophore of a Cph2-like phytochrome. *Journal of Physical Chemistry B, 124*(33), 7115–7127. https://doi.org/10.1021/acs.jpcb.0c03431

50. Rumfeldt, J. A., Takala, H., Liukkonen, A., & Ihalainen, J. A. (2019). UV-Vis spectroscopy reveals a correlation between Y263 and BV protonation states in Bacteriophytochromes. *Photochemistry and Photobiology, 95*(4), 969–979. https://doi.org/10.1111/php.13095

51. Velazquez Escobar, F., Lang, C., Takiden, A., Schneider, C., Balke, J., Hughes, J., Alexiev, U., Hildebrandt, P., & Mroginski, M. A. (2017). Protonation-dependent structural heterogeneity in the chromophore binding site of Cyanobacterial phytochrome Cph1. *The Journal of Physical Chemistry B, 121*(1), 47–57. https://doi.org/10.1021/acs.jpcb.6b09600

52. Wagner, J. R., Zhang, J., Von Stetten, D., Günther, M., Murgida, D. H., Mroginski, M. A., Walker, J. M., Forest, K. T., Hildebrandt, P., & Vierstra, R. D. (2008). Mutational analysis of Deinococcus radiodurans bacteriophytochrome reveals key amino acids necessary for the photochromicity and proton exchange cycle of phytochromes. *Journal of Biological Chemistry, 283*(18), 12212–12226. https://doi.org/10.1074/jbc.M709355200

53. Hahn, J., Strauss, H. M., Landgraf, F. T., Gimenez, H. F., Lochnit, G., Schmieder, P., & Hughes, J. (2006). Probing protein-chromophore interactions in Cph1 phytochrome by mutagenesis. *FEBS Journal, 273*(7), 1415–1429. https://doi.org/10.1111/j.1742-4658.2006.05164.x

54. Burgie, E. S., Bussell, A. N., Walker, J. M., Dubiel, K., & Vierstra, R. D. (2014). Crystal structure of the photosensing module from a red/far-red light-absorbing plant phytochrome. *Proceedings of the National Academy of Sciences of the United States of America, 111*(28), 10179–10184. https://doi.org/10.1073/pnas.1403096111

Authors and Affiliations

Tobias Fischer[1] · Lisa Köhler[2] · Tanja Ott[1] · Chen Song[2] · Josef Wachtveitl[1] · Chavdar Slavov[1]

Tobias Fischer
fischer@theochem.uni-frankfurt.de

Lisa Köhler
l.koehler@uni-leipzig.de

Tanja Ott
ott@chemie.uni-frankfurt.de

Chen Song
chen.song@uni-leipzig.de

[1] Institute of Physical and Theoretical Chemistry, Goethe University Frankfurt Am Main, Max-von-Laue-Straße 7, 60438 Frankfurt, Germany

[2] Institute for Analytical Chemistry, University of Leipzig, Linnéstraße 3, 04103 Leipzig, Germany